

Integrating Hybrid Supercapacitors With Batteries: Unravelling the Mechanism in Zn-I₂/MnO₂ Systems

Zanxiang Nie¹, Guodong Fu², Kwun Nam Hui³, Kwan San Hui⁴, Senior Member, IEEE, Pritesh Hiralal⁵, Gehan A.J. Amaratunga⁶, Yue Liu⁷, Yaotang Zhong⁸, Shiwei Liu⁹, and Shiqiang Luo¹⁰, Member, IEEE

Abstract—Supercapatteries, integrating supercapacitors and batteries, offer a promising route to combine high power and energy density. This study decouples their charging behavior by constructing hybrid (Zn//AC) and symmetric (AC//AC) supercapacitors coupled with I₂/MnO₂ batteries. We identify a stepwise mechanism where supercapacitor charging precedes battery reactions. The Zn//AC configuration successfully integrates with the I₂ battery, while the symmetric AC//AC system fails due to the shuttle effect. The zinc anode enables both efficient capacitive charging and stable battery operation. Furthermore, charge transfer between the supercapacitor and battery subsystems is observed, highlighting their dynamic interplay. These findings provide key insights for designing integrated, high-performance energy storage systems with tunable capacitive and battery-like behavior.

Index Terms—Charge transfer, hybrid supercapacitor, iodine battery, stepwise charging, supercapattery, zinc anode.

I. INTRODUCTION

BY INTEGRATING batteries and supercapacitors, the “supercapattery” demonstrates the potential to unlock the advantages of battery–supercapacitor hybrid systems [1], offering more possibilities for incorporating energy storage and conversion systems into electronic devices. Supercapacitors (SCs) based on the electric double-layer capacitor (EDLC) mechanism exhibit excellent power density and cycling stability, but are typically limited by their low energy density [2]. To enhance the energy density of SCs, faradaic charge storage mechanisms—which can be capacitive (pseudocapacitive) or non-capacitive

Received 21 October 2025; revised 8 January 2026; accepted 4 February 2026. Date of publication 9 February 2026; date of current version 20 February 2026. This work was supported in part by the Shenzhen Science and Technology Program under Grant SZXJP20230703093207017, Grant KJZD20230923113759002, and Grant KQTD20190929172522248, in part by the Guangdong Introducing Innovative and Entrepreneurial Teams Program under Grant 2019ZT08Z656, and in part by the Shenzhen Association for Science and Technology. The review of this article was arranged by Editor P. Feng. (Corresponding authors: Shiqiang Luo; Shiwei Liu.)

Zanxiang Nie, Pritesh Hiralal, Gehan A.J. Amaratunga, Yaotang Zhong, Shiwei Liu, and Shiqiang Luo are with Zinergy Shenzhen Ltd., AI Digital Valley, Shenzhen 518109, China (e-mail: liushiwei@zinergy-power.cn; luoshiqiang@zinergy-power.cn).

Guodong Fu and Kwun Nam Hui are with the Institute of Applied Physics and Materials Engineering, University of Macau, Macau 999079, China.

Kwan San Hui is with the Department of Mechanical Engineering, Prince Mohammad Bin Fahd University, Al Khobar 31952, Saudi Arabia.

Yue Liu is with the School of Internet of Things, Xi’an Jiaotong-Liverpool University, Suzhou 215123, China.

This article has supplementary downloadable material available at <https://doi.org/10.1109/TMAT.2026.3662625>, provided by the authors.

Digital Object Identifier 10.1109/TMAT.2026.3662625

(battery-like)—have been introduced [3]. A typical example is the hybrid supercapacitor, in which one electrode is replaced by a battery-type electrode while the other remains an EDLC-based SC electrode. Going a step further, integrating EDLC-based SCs with battery electrode materials leads to the formation of a supercapattery [4], [5]. This can be achieved either by incorporating redox-active materials into the electrodes or by using redox-active electrolytes [6], [7].

One advantage of using redox electrolytes in supercapatteries is that the configuration of conventional SCs does not need to be altered—only the electrolyte needs to be modified. Another benefit is that the charging and discharging processes of the SC part and the battery part interfere less with each other within the integrated device. Unlike charge adsorption at the electrode–electrolyte interface, which can occur over a wide potential range, battery reactions require a specific redox potential and often result in a voltage plateau [5]. In other words, integrating a battery system can enhance capacity without the need to widen the electrochemical window of the electrolyte. Moreover, if excess redox species are present in the electrolyte, the reaction potential of the battery can set an upper voltage limit, thereby preventing overcharging. Although the voltage curves of our supercapacitor resemble those of underpotential deposition pseudo capacitance, where metal ions or hydrogen form an adsorbed monolayer on the surface of a noble metal well above their redox potential [1], the behavior observed in this work is quite different. This is because the voltage plateau originates from the deposition of oxides such as I₂ and MnO₂. Furthermore, this work provides an in-depth explanation of the charge-transfer mechanism between symmetric/hybrid supercapacitors and the I₂/MnO₂ battery system, in which MnO₂ was first reported in our previous work via electrolytic deposition on activated carbon [5], [8].

To realize these advantages, this study decouples the charging mechanisms in supercapatteries by integrating hybrid or symmetric supercapacitors with I₂/MnO₂ battery systems. We reveal a stepwise charging process in which SC charging occurs prior to battery reactions. Importantly, the Zn//AC hybrid supercapacitor couples successfully with the I₂ battery, whereas the AC//AC symmetric supercapacitor fails due to the shuttle effect. The zinc anode facilitates both low-voltage SC charging and stable battery operation. This work offers fundamental insights for designing integrated, high-performance energy storage systems.

II. EXPERIMENTAL SECTION

A. Materials

Zinc acetate ($\text{ZnAc}_2 \cdot 2\text{H}_2\text{O}$, 99%), manganese acetate tetrahydrate ($\text{MnAc}_2 \cdot 4\text{H}_2\text{O}$, 99%), zinc iodide (ZnI_2 , 98%), and potassium iodide (KI, $\geq 99\%$) were purchased from Aladdin (Shanghai). Potassium chloride (KCl, 99.5%) was obtained from Macklin. Activated carbon (specific surface area: $1800 \text{ m}^2/\text{g}$) was supplied by XFNANO Ltd. The thin-film carbon and zinc electrodes were fabricated by Zinergy Shenzhen Ltd. using a screen-printing method. Polyethylene terephthalate (PET) was used as the substrate for the thin-film electrodes. The printable carbon paste was prepared by mixing graphite, carbon black, a polymer binder, and a solvent. The zinc paste was prepared by mixing zinc powder with carbon black, a polymer binder, and a solvent. After screen printing, the carbon and zinc pastes were annealed at 100°C for 10 and 20 minutes, respectively. The zinc paste was printed onto pre-annealed carbon layers. The thicknesses of the carbon and zinc layers were controlled at $10 \mu\text{m}$ and $50 \mu\text{m}$, respectively.

B. Device Fabrication and Characterization

For the activated carbon layer, poly (vinylidene fluoride), Super-P carbon black, and activated carbon in a mass ratio of 1:1:8 were mixed in N-methyl-2-pyrrolidone. The resulting activated carbon paste was then coated onto the thin-film carbon electrodes with mass loadings of $1 \text{ mg}/\text{cm}^2$ or $3 \text{ mg}/\text{cm}^2$, followed by drying in a vacuum oven at 80°C for 5 hours.

For the thin-film devices, filter paper (thickness: 0.17 mm) was used as a separator between the positive and negative electrodes. The active electrode area was $4 \times 2.5 \text{ cm}^2$, and $250 \mu\text{L}$ of electrolyte ($1 \text{ M ZnAc}_2 + 2 \text{ M KCl} + 2 \text{ M KI}$ or 1 M MnAc_2 , typically) was added before sealing.

Charge and discharge curves were recorded using a LANHE CT3002AU battery test system. Unless otherwise specified, the galvanostatic charge-discharge was performed by charging to a fixed capacity of 2 mAh and then discharging to a cutoff voltage of 0 V , both at a current of 2 mA .

III. RESULTS AND DISCUSSION

A. Different Charging Mechanisms

When charging a capacitor, the capacitance (C) can be considered constant, as it is determined by intrinsic properties such as surface area, plate distance, and dielectric constant. In a symmetrical supercapacitor (SC) based on the electric double-layer capacitor (EDLC) mechanism, the capacity (Q) increases linearly with voltage (V): $Q = C \times V$. In a hybrid supercapacitor, one electrode resembles that of an EDLC-type SC, while the other is a battery-type electrode. For instance, a typical zinc hybrid supercapacitor consists of a metallic zinc anode and an activated carbon (AC) cathode. Because the conductive zinc metal enables extensive zinc ion plating, the overall capacity is limited by the AC cathode. As shown in Figure S1, the SC capacity does not originate from graphite carbon or the zinc anode.

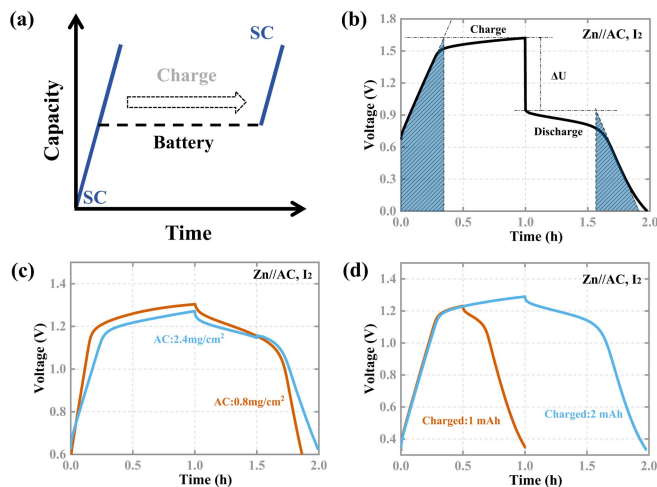


Fig. 1. (a) Schematic diagram of the stepwise charging mechanism of the supercapattery. (b) Analysis of a typical charge-discharge voltage curve for a zinc/activated carbon (Zn//AC) hybrid supercapacitor with a battery-type electrolyte ($1 \text{ M ZnAc}_2 + 2 \text{ M KI} + 2 \text{ M KCl}$). Charge-discharge voltage curves of the Zn//AC, I_2 -based supercapattery under different conditions: (c) with the same charging capacity (2 mAh) but different AC mass loadings (0.8 and $2.4 \text{ mg}/\text{cm}^2$), and (d) with the same AC mass loading ($0.8 \text{ mg}/\text{cm}^2$) but different charging capacities (1 and 2 mAh).

However, when charging a battery, the voltage must exceed the redox reaction potential, resulting in a relatively flat voltage plateau. Therefore, in a supercapattery (i.e., a combined supercapacitor and battery) as illustrated in Fig. 1(a), the device initially behaves like a supercapacitor until the voltage reaches the redox potential of the battery component. Once this potential is reached and before the reactants are depleted, the device operates in battery mode. After reactant depletion, it reverts to supercapacitor behavior. Detailed reaction processes are discussed in Fig. S2. In this configuration, the AC serves not only as a supercapacitor electrode for charge adsorption but also as a current collector for deposited battery cathode materials such as I_2 or MnO_2 .

As a typical example, Fig. 1(b) displays the constant-current charge and discharge voltage curves for a supercapattery with a zinc metal anode, an activated carbon (AC) cathode, and an electrolyte containing zinc and iodide ions (denoted as Zn//AC, I_2). Under galvanostatic conditions, capacity increases linearly with charging time according to $Q = I \times t$. Initially, the voltage rises linearly, consistent with the mechanism in Fig. 1(a). The voltage then increases more slowly as it approaches the reaction potential for oxidizing I^- to I_2 . As the I^- concentration decreases, the battery charging voltage also rises slightly. Because this voltage increase also contributes to the supercapacitor (SC) capacity, the sloped voltage line representing the SC is extended to the end of the charging period. Thus, the SC contribution to the total capacity can be estimated from the straight left edge of the trapezoidal region. Similarly, during discharge, the SC contribution can be estimated from the base of the triangular region on the right, where the slope is defined by the steepest part of the discharge curve.

It should be noted that the devices are fabricated on thin-film substrates using large-area graphite carbon as the current

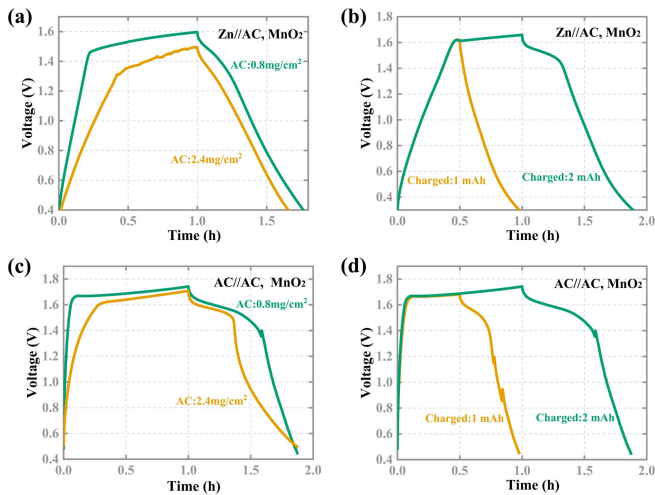


Fig. 2. Charge-discharge voltage curves of the MnO₂-based supercapattery for hybrid supercapacitor electrodes (Zn//AC) in (a, b) and for symmetric supercapacitor electrodes (AC//AC) in (c, d), which are tested under the following conditions: (a) and (c) at a fixed charging capacity (2 mAh) but with different AC mass loadings (0.8 and 2.4 mg/cm²); (b) and (d) at a fixed AC mass loading (0.8 mg/cm²) but with different charging capacities (1 and 2 mAh). The electrolyte was 1 M ZnAc₂ + 1 M MnAc₂ + 2 M KCl.

collector, as shown in Fig. S3. The significant internal resistance causes a voltage gap (ΔU) when switching between charging and discharging modes. This voltage gap can be used to estimate the internal resistance as $R_i = \Delta U / \Delta I$. To mitigate the influence of internal resistance, the voltage curves in the main text have been IR-compensated. This was done by subtracting half of the Ohmic drop ($\Delta U/2$) during the charging phase and adding half ($\Delta U/2$) during the discharging phase, given that the charge and discharge currents were of equal magnitude, which was 2 mA in all standard tests. The original, unadjusted curves are provided in the supplemental file.

To further demonstrate the stepwise charging mechanism, we modulated the capacitance and battery charging capacity by increasing the amount of AC and the charging time, respectively, as shown in Fig. 1(c), (d), and S4.

In Fig. 1(c), increasing the AC mass loading from 0.8 to 2.4 mg/cm² reduces the voltage slope, consistent with the equation $V = (I \times t) / C$, since capacitance C increases with AC surface area. As the charging voltage reaches the battery reaction potential later, the supercapacitor (SC) contributes more to the total capacity. In Fig. 1(d), increasing the charging time enhances the battery contribution, while the voltage slope associated with the SC part remains unchanged.

Besides the higher battery reaction potential, the above conclusions also hold for a supercapattery using MnO₂ as the cathode material for the battery component, as shown in Fig. 2 and S5. Fig. 2(a) and (b) present the hybrid supercapattery (Zn//AC, MnO₂), while Fig. 2(c) and (d) show the symmetric supercapattery (AC//AC, MnO₂). The different anode materials in the symmetric and hybrid configurations lead to different response speeds, as seen when comparing Fig. 2(b) and (d). Due to the faster response of the EDLC compared to zinc deposition at the anode for charge accumulation, the charging

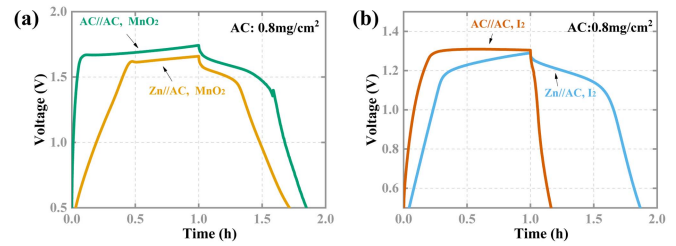


Fig. 3. Charge-discharge voltage curves comparing four different device configurations. The configurations combine either AC//AC (symmetric supercapacitor) or Zn//AC (hybrid supercapacitor) electrodes with MnO₂ or I₂-based cathodes. (a) Comparison between AC//AC, MnO₂ and Zn//AC, MnO₂ devices. (b) Comparison between AC//AC, I₂ and Zn//AC, I₂ devices. All tests were performed with a fixed AC mass loading of 0.8 mg/cm² and a fixed charging capacity of 2 mAh.

voltage increases more gradually in the hybrid supercapattery in Fig. 2(b). Interestingly, in Fig. 2(a), increasing the AC content not only enhances the SC contribution but also lowers the battery reaction potential. This may be due to the facilitation of charge transfer from the supercapacitor to the battery subsystem by the enhanced SC capability.

B. The Influence of SC Systems on Battery Systems

To enable clearer comparison, Fig. 3 and S6 present all four combinations of supercapacitors (SCs) and batteries. For the MnO₂-based supercapattery, the symmetric SC-based device shows a higher battery charging voltage and greater battery capacity contribution than the hybrid SC-based system, as the voltage rises more rapidly during the SC phase.

In contrast, for the AC//AC, I₂-based supercapattery, although a voltage plateau indicative of battery charging appears, no corresponding battery discharge is observed, and the device functions similarly to a symmetric SC alone. This malfunction of the I₂ battery component is caused by the well-known iodine shuttle effect, which will be discussed later.

Using the method from Fig. 1(b), the capacity composition of each system is analyzed in Figs. 4 and 5. For Zn//AC, I₂ supercapattery, while the SC subsystem experiences a slight drop in discharge capacity, the battery subsystem's charge/discharge capacities are almost unchanged. The stable capacity ratio between them is likely due to the fast reaction dynamics shown in Fig. S7. For AC//AC, I₂ supercapattery, however, the stable SC performance contrasts with a marked battery imbalance—increased charging capacity yields minimal discharge recovery (Fig. S8). This contrast partially confirms the presence of iodine shuttle reactions.

For both MnO₂ based supercapatteries, the sluggish battery discharging reaction were observed in Fig. S9 and S10, which would be due to the two-step electron transfer during MnO₂ discharge ($Mn^{2+} \rightarrow Mn^{4+}$ during charging, and $Mn^{4+} \rightarrow Mn^{3+} \rightarrow Mn^{2+}$ during discharging) [9]. However, while the battery discharging capacity exceeds the battery charging capacity in the Zn//AC, MnO₂ supercapattery, the opposite trend is seen in the AC//AC, MnO₂ systems with the SC discharging capacity exceeds the SC charging capacity.

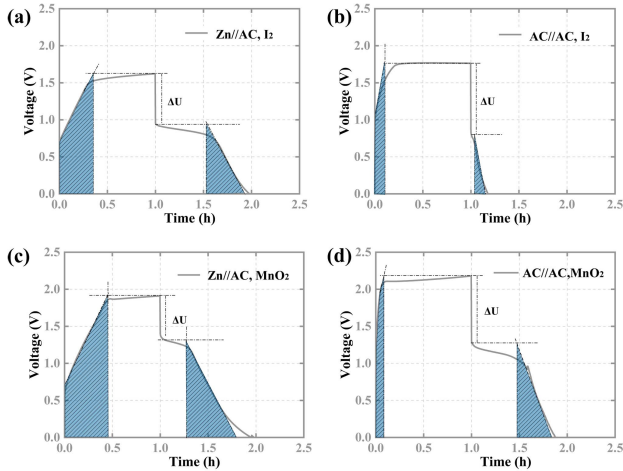


Fig. 4. Analysis of the uncompensated charge-discharge voltage curves from Fig. 3, showing the voltage gap due to internal resistance. The capacitive and battery-like capacity components during charging and discharging were quantified using the method outlined in Fig. 1(b). Specifically, the widths of the left trapezoid and the right triangle represent the supercapacitor's contribution to the charging and discharging capacities, respectively. The battery capacity was then calculated by subtracting these supercapacitor components from the total capacity.

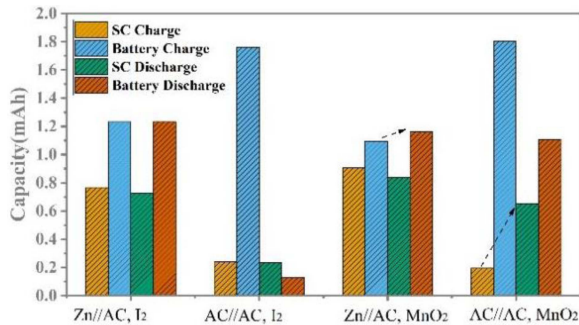


Fig. 5. Quantitative distribution of the capacity contributions from the supercapacitor and battery, as determined from the data in Fig. 4.

The proposed charge transfer mechanism is illustrated in Fig. S11. During charging, the supercapacitor (SC) subsystem responds faster than the battery subsystem. This differential response creates an overpotential that drives charge transfer from the SC to the battery. During discharging, the overpotential reverses direction (now on the battery side), driving charge from the battery back to the SC. A residual overpotential at the end of charging can also facilitate additional SC-to-battery charge transfer.

Due to its higher capacitance, the Zn//AC configuration exhibits more charge transfer than AC//AC during charging process. However, during discharging, the faster reaction kinetics of AC//AC lead to a rapid voltage drop, which promotes a larger amount of charge transfer from the battery to the SC. The fact that the I_2 reaction is faster than that of MnO_2 , resulting in less charge transfer, is also consistent with the above explanation.

C. The Combination of Hybrid SC With I_2 Battery

The successful integration of a hybrid supercapacitor (SC) with an I_2 battery, in contrast to the failure of integrating an

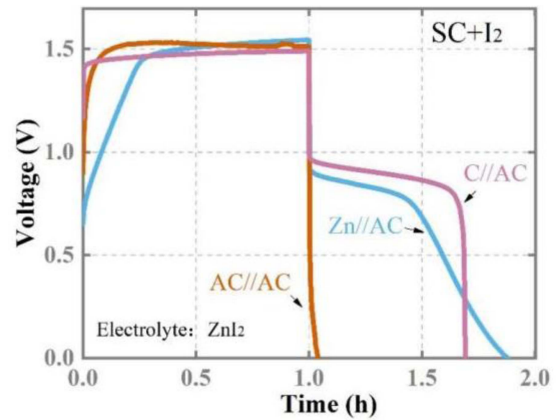


Fig. 6. Charge-discharge voltage curves of I_2 -based supercapatteries employing different supercapacitor electrode pairs: AC//AC, Zn//C, and graphite carbon//activated carbon (C//AC). The electrolyte was 2 M ZnI_2 . All tests were performed with a fixed AC mass loading of 0.8 mg/cm^2 and a fixed charging capacity of 2 mAh.

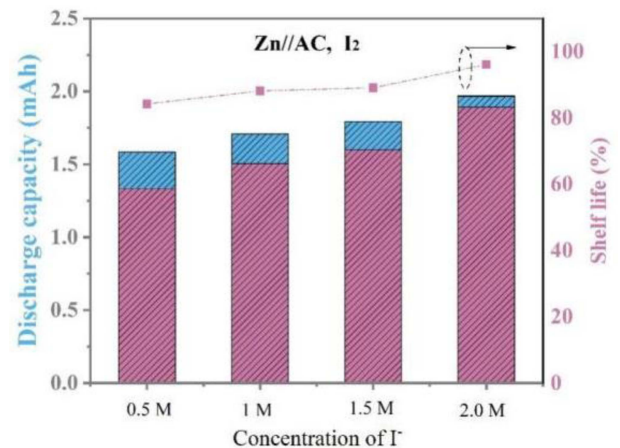


Fig. 7. Discharge capacities of the supercapatteries after a 2 mAh charge, and the retained capacities after a subsequent 1-hour rest period. The percentages of retained capacity indicate the devices' capacity retention (or self-discharge behavior) after 1 hour of rest. All devices used Zn//AC electrodes and electrolytes of $1 \text{ M } ZnAc_2 + 2 \text{ M } KCl + x \text{ M } KI$, with x varying as 0.5, 1.0, 1.5, and 2.0.

electric double-layer capacitor (EDLC) SC with an I_2 battery, led us to further investigate the underlying mechanism. To simplify the systems, the electrolyte was replaced with ZnI_2 only. As shown in Fig. 6 and S12, the discharge capacities maintain the trend: Zn//AC > C//AC > AC//AC.

Since charging plateaus corresponding to the Zn- I_2 battery are observed, we can rule out insufficient voltage or adsorption of other cations at the anode side hindering zinc plating as causes of failure. Comparing the Zn//AC and C//AC cases, the presence of zinc not only facilitates charging of the hybrid SC at low voltage but also promotes the deposition of metallic zinc. As a result, clear SC behavior is observed, and a higher overall discharge capacity is achieved.

We further studied the shuttle effect by allowing charged devices to stand for 1 hour and then measuring the remaining discharge capacity, as shown in Fig. 7 and S13. The shelf life improves with increasing iodide concentration up to an optimal value. This optimal concentration is identified in Fig.

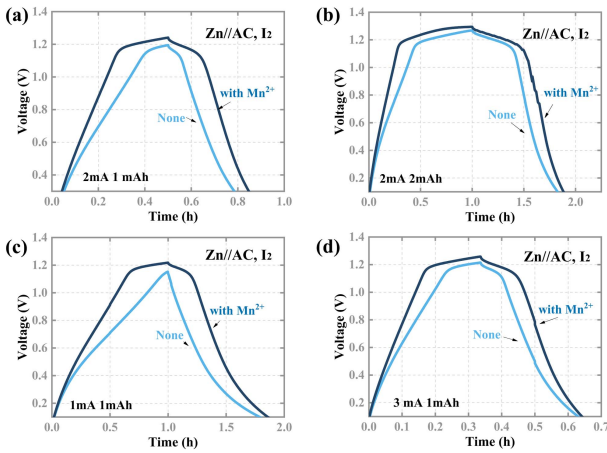


Fig. 8. Charge-discharge voltage curves comparing the performance of Zn//AC, I₂-based supercapatteries with electrolytes containing 1 M ZnAc₂ + 2 M KI + 2 M KCl, with and without 0.2 M MnAc₂ additive. The devices were systematically evaluated under the following conditions: (a), (b) Constant current (2 mA) at charging capacities of 1 and 2 mAh; (c), (a), (d) Constant charging capacity (1 mAh) at currents of 1, 2, and 3 mA.

S14. Furthermore, the unchanged SC discharge capacity despite extended battery charging (Fig. S7b) suggests that accumulated positive charges drive the electrostatic adsorption of I³⁻ at the cathode [5]. However, this beneficial adsorption is limited by the SC's finite charge capacity. Therefore, above the optimal concentration, the aggravated shuttle reactions cannot be fully counteracted, causing performance to decline.

However, in the AC//AC, I₂-based supercapattery, the concentration of positive charge at the anode–electrolyte interface may weaken this electrostatic adsorption at the cathode (Fig. S15). Moreover, the higher specific surface area of the AC anode exacerbates side reactions between metallic zinc and I₃⁻.

To verify the adsorption of I₃⁻, I₂-based supercapatteries with C//AC and AC//AC electrode configurations were assembled and tested in cuvette cells (Fig. S16). A graphite anode was employed instead of zinc to avoid additional reduction of the generated I₃⁻. The observation of a yellowish precipitate confirmed the formation of I₃⁻, thereby validating the operation of the I₂ battery subsystem in the AC//AC supercapattery.

Benefiting from I₃⁻ adsorption, the Zn//AC, I₂ supercapattery demonstrates superior cycling performance compared to MnO₂-based devices. In contrast to the challenging iodide shuttle effect, zinc dendrites are a less critical issue (Fig. S17). This failure of MnO₂-based supercapatteries is attributed to device inflation resulting from hydrogen evolution, as shown in Fig. S18. Notably, using simple untreated AC electrodes and our optimized electrolyte, we achieve performance on par with literature reports that rely on doped or complex structured AC electrodes (Fig. S19).

D. Adding Mn²⁺ Into Zn//AC, I₂-Based Supercapattery

Because the oxidation potential of I₂ is lower than that of MnO₂, as shown in Fig. S2, the I₂ battery charging process is triggered before that of the MnO₂ battery in a supercapattery containing both I⁻ and Mn²⁺ in the electrolyte [10], [11]. As

shown in Fig. S20, an excess of I⁻ completely inhibits MnO₂ deposition. Thus, in our previous report [5], we used I⁻ to recycle the peeled-off “dead” MnO₂ in a Zn//AC, MnO₂-based supercapattery, which improved both cycling performance and Coulombic Efficiency. Here, we apply the previously discussed charging mechanism to a specific case involving the addition of Mn²⁺ to a Zn//AC, I₂-based supercapattery.

As shown in Fig. 8 and S21, after adding Mn²⁺, the SC charging contribution decreases while the battery charging contribution increases, leading to a higher average discharge voltage. When the charging current is reduced to 1 mA, as shown in Fig. 8(c), the device even transitions from a hybrid supercapattery to a supercapattery. This transformation is likely driven by the facilitated oxidation of I⁻ at the cathode, which promotes the device's transition into battery mode, as revealed in the CV curves of Figs. S22. With this result, we complete the final piece of the overall picture of the four systems, building on our earlier reports [5], [12].

IV. CONCLUSION

In this work, we have decoupled the complex charging processes in supercapatteries and established a general stepwise mechanism. Through a side-by-side comparison of four integrated systems, we demonstrate that the successful coupling of a battery component with a supercapacitor is highly dependent on the SC's architecture. The hybrid Zn//AC configuration is uniquely advantageous, as the zinc anode facilitates both rapid capacitive charging and stable battery operation, effectively integrating the I₂ battery and suppressing the shuttle effect through interfacial electrostatic adsorption. The observed charge transfer between SC and battery subsystems further underscores the dynamic interplay within these hybrid devices. The ability to tune the device's behavior—from capacitor-like to battery-like—by simply adjusting the current or adding active ions like Mn²⁺, highlights the design flexibility of the supercapattery concept. This work not only clarifies the underlying mechanisms governing integrated SC-battery systems but also provides a clear guideline for future material selection and device engineering towards high-performance, multi-functional energy storage.

ACKNOWLEDGMENT

Dr. Shiqiang Luo would like to thank Prof. Xihong Lu at Sun Yat-Sen University, Prof. Buddha Deka Boruah and Prof. Georgios Nikiforidis at University College London, and Prof. Manish Chhowalla and Prof. Yan Wang at the University of Cambridge for hosting his visit and for the fruitful discussions.

REFERENCES

- [1] S. Seenivasan, S. Adhikari, A. T. Sivagurunathan, and D. Kim, “Supercapatteries: Unlocking the potential of battery-supercapacitor fusion,” *Energy Environ. Sci.*, vol. 18, pp. 1054–1095, 2025.
- [2] C. Wang, X. Zeng, P. J. Cullen, and Z. Pei, “The rise of flexible zinc-ion hybrid capacitors: Advances, challenges, and outlooks,” *J. Mater. Chem. A*, vol. 9, pp. 19054–19082, 2021.
- [3] L. Yu and G. Z. Chen, “Redox electrode materials for supercapatteries,” *J. Power Sources*, vol. 326, pp. 604–612, 2016.

- [4] D. P. Dubal, O. Ayyad, V. Ruiz, and P. Gómez-Romero, "Hybrid energy storage: The merging of battery and supercapacitor chemistries," *Chem. Soc. Rev.*, vol. 44, pp. 1777–1790, 2015.
- [5] S. Liu, S. Luo, G. A. J. Amaratunga, P. Hiralal, and Z. Nie, "Thin-film flexible zinc hybrid electrochemical device integrating three chemical pathways," *J. Power Sources*, vol. 614, 2024, Art. no. 235045.
- [6] B. Akinwolemiwa, C. Peng, and G. Z. Chen, "Redox electrolytes in supercapacitors," *J. Electrochem. Soc.*, vol. 162, 2015, Art. no. A5054.
- [7] K. Fic, E. Frackowiak, and F. Béguin, "Unusual energy enhancement in carbon-based electrochemical capacitors," *J. Mater. Chem.*, vol. 22, pp. 24213–24223, 2012.
- [8] S. Liu et al., "Recent progress in cathode-free zinc electrolytic MnO₂ batteries: Electrolytes and electrodes," *Batteries*, vol. 11, 2025, Art. no. 171.
- [9] D. L. Chao et al., "An electrolytic Zn-MnO₂ battery for high-voltage and scalable energy storage," *Angewandte Chemie-Int. Ed.*, vol. 58, pp. 7823–7828, 2019.
- [10] J. F. Lei, Y. X. Yao, Z. Y. Wang, and Y. C. Lu, "Towards high-areal-capacity aqueous zinc-manganese batteries: Promoting MnO₂ dissolution by redox mediators," *Energy Environ. Sci.*, vol. 14, pp. 4418–4426, 2021.
- [11] C. X. Xie, T. Y. Li, C. Z. Deng, Y. Song, H. M. Zhang, and X. F. Li, "A highly reversible neutral zinc/manganese battery for stationary energy storage," *Energy Environ. Sci.*, vol. 13, pp. 135–143, 2020.
- [12] S. Liu, S. Luo, G. Yang, and Z. Nie, "Integrating zinc iodine battery with zinc hybrid capacitor in one cell," *J. Phys.: Conf. Ser.*, vol. 2809, 2024, Art. no. 012035.